

Adsorption Sites and Diffusion Rates of Benzene in HY Zeolite by Force Field Based Simulations

Fabien Jousse,^{*,†,‡} Scott M. Auerbach,[‡] and Daniel P. Vercauteren[†]

Computational Chemical Physics Group, Institute for Studies in Interface Science, Facultés Universitaires Notre-Dame de la Paix, Rue de Bruxelles 61, B-5000 Namur, Belgium, and Department of Chemistry and Department of Chemical Engineering, University of Massachusetts, Amherst, Massachusetts 01002

Received: October 6, 1999; In Final Form: December 15, 1999

A variety of force field based simulations have been used to study the location and diffusion of benzene adsorbed in a model zeolite HY (Si/Al = 2.43), namely: molecular docking; equilibrium and nonequilibrium molecular dynamics; and Monte Carlo umbrella sampling. Multiple adsorption sites are found, with benzene facially coordinated to one or two H(1) or H(2) protons in the supercage. Some slight adsorption onto the 12-membered ring windows is also observed, in accordance with infrared measurements. The minimum energy path at low temperature proceeds via a creeping of the molecule along the zeolite wall between stable sites, with an activation energy varying between 10 and 20 kJ mol⁻¹. This type of creeping motion is observed both for intracage and intercage diffusion. Cartwheel jumps between sites are seen to proceed with higher activation energies of approximately 30 kJ mol⁻¹. Multiple paths from site to site open as the temperature increases. This results in a strong temperature dependence of the potential of mean force in the zeolite cage, as calculated by umbrella sampling. Nonequilibrium molecular dynamics simulations initialized at the transition state between two states show that the molecules do not relax in a single final state but in a multiplicity of states; only cage-to-cage jumps keep a sense, as a majority of molecules relax in the final cage. Due to the multiplicity of possible cage-to-cage paths, the temperature dependence of the cage-to-cage rate constants is deeply non-Arrhenius.

1. Introduction

Many experimental and theoretical studies have focused on benzene adsorbed into siliceous or cationic faujasite. We feel that knowledge of these systems is, if not perfect, at least a good way to completion. Force field based simulations^{1–7} as well as Ising models^{8–13} have helped us to understand their behavior. As an example, the theoretical prediction of the activation energy of self-diffusivity of benzene in NaY was experimentally confirmed¹⁴ after publication of the simulation results.³

The situation is quite different with acidic faujasites. Indeed, only a few studies ventured to investigate adsorption and diffusion of benzene in HY by gravimetry,¹⁵ neutron diffraction and molecular mechanics,^{16,17} infrared spectroscopy,^{18,19} NMR^{20,21} or density functional theory.²¹ It is quite clear that computational studies of benzene in HY are much more complex than in siliceous or even cationic faujasites. The mechanism of proton transfer between the guest molecule and the host structure needs to be treated at the ab initio level,²¹ but the same level of theory cannot yet allow to compute the diffusivity of the guest molecules in the structure. Jump diffusion models (JDM) or kinetic Monte Carlo (KMC) approaches offer a way to overcome this difficulty. Indeed, these techniques represent the diffusion of the guest molecule as a series of random jumps between definite adsorption sites.^{13,22,23} Proton transfer can easily be included by adding other types of “virtual jumps” corresponding to the actual chemisorption and reaction rates.^{24,25} If the latter

rates still need to be computed with ab initio methods, all rates corresponding to physisorbed processes only require force field based atomistic simulations. Consequently, if the diffusion proceeds by jumps between sites where benzene is physisorbed, force field based simulations would suffice to compute the actual diffusion rates; however, if diffusion proceeds by proton-assisted hopping processes between sites where benzene is chemisorbed, then the diffusion rates also need to be computed using ab initio methods. Contrarily to HSAPO37,^{16,18,19} no redistribution of the protons upon benzene adsorption was observed in HY.^{17–19} This observation strongly suggests that the main diffusion mechanism is due to the hopping between physisorbed sites.

The above-mentioned reasons clearly show the interest of force field based determinations of the physisorption sites and hopping rates of benzene in HY. In the present article, we will present results of such calculations, for future use in a KMC type simulations.¹³ A variety of different force field based molecular modeling techniques have been applied, namely: molecular docking, equilibrium and nonequilibrium molecular dynamics, constrained minimization along a “reaction path,” and Monte Carlo umbrella sampling. We will show that a variety of adsorption sites exist in HY, where benzene is facially coordinated to one or two protons; that diffusion of benzene at 0 K proceeds via “creeping” along the zeolite wall between these sites, even during the cage-to-cage jumps; that at higher temperatures the existence of multiple pathways between the sites prevents the calculation of any site-to-site rate coefficient, so that the only meaningful motion on larger time scales is the cage-to-cage hop.

In the next section, we will review the experimental and theoretical knowledge of benzene adsorption in HY, and detail

* Corresponding author Email: fjousse@scf.fundp.ac.be.

† Facultés Universitaires Notre-Dame de la Paix.

‡ University of Massachusetts.

the zeolite structure used in the study. The third section will be dedicated to the computational methods considered: we will describe the derivation of the force field and the techniques used to determine the adsorption sites and compute the diffusion rates. In a fourth section we will present the results of the calculation and a relevant discussion, with comparison to relevant experimental data.

2. HY Structure With and Without Sorbed Benzene

HY is a FAU-type zeolite with protons compensating some or all the negative charges of the framework.²⁶ There is no particular ordering of the aluminum in the framework, apart from Löwenstein's rule,²⁷ in accordance to what is observed in NaX and NaY.²⁸ The main question comes from the distribution and location of the protons. The crystal structure from X-ray diffraction only gives indirect evidence of the proton positions.²⁹ Neutron diffraction studies allow us to locate them more directly.^{17,30,31} In all cases the protons were found to be preferentially linked to O(3) and O(1), then to O(2), and finally to O(4). The exact repartition between these sites depends on the composition of the sample: Jiráček et al.³⁰ found 21.1 ± 5.5 H(1), 30.9 ± 7.0 H(3), and no H(2) or H(4) per unit cell; Czjzek et al.³¹ found 28.6 ± 1.0 H(1), 15.0 ± 1.0 H(3), 9.5 ± 1.0 H(2) and no H(4) per unit cell; Vitale et al.¹⁷ observed about 22 H(3), 13 H(1), 3 H(2), and 4 H(4). The latter group also notes that the distribution of the protons remains unchanged upon adsorption of benzene. This is in contrast to what is observed in HSAPO-37, which has the same faujasite structure: in this aluminophosphate the protons are seen to redistribute over O(2) upon adsorption of benzene.³² Infrared spectroscopy confirms the redistribution of the protons in HSAPO-37 but not in HY.¹⁸

Infrared studies, beginning with Jacobs and Uytterhoeven in 1973,³³ have shown that there are two bands corresponding to O–H vibration in HY: a narrow high frequency (HF) band, and a broad low frequency (LF) band. The usual explanation is that protons linked to O(1) and O(2) point in the supercage and are responsible for the narrow HF component, while protons at O(3) and O(4) point inside the smaller sodalite cages, where H-bonding with the framework oxygens broadens the corresponding infrared band; see, e.g., van Santen and Kramer³⁴ and references therein. Observations of the bending mode of the protons,³⁵ as well as computer simulations of the vibrational frequencies,³⁶ seem in broad accordance with this view. Note that Datka et al.^{37,38} proposed another explanation: the two bands would be due to framework oxygen atoms in different environments, namely Si(4Al), Si(3Al), Si(2Al), and Si(1Al). This explanation is based on the observation of a single narrow HF component in NaX(Si/Al = 1), where there is also only one type of environment Si(4Al). However, in a recent paper by Sierka et al.,³⁹ it is shown by mixed quantum/classical simulations that although the acidity of the proton sites in HY depends on the number of neighboring Al sites, it is not the case for the infrared frequency or the NMR shift, which invalidates the picture proposed earlier by Datka et al.^{37,38}

Barthomeuf and Ha^{40,41} have studied the adsorption of benzene in Na₅₆HY(Si/Al = 2.43) by calorimetry and found that the heat of adsorption decreases when increasing the number of protons: while in Na₅₆Y the heat of adsorption reaches 79 kJ mol⁻¹, for a structure with 8.7 Na and 47.3 H per unit cell the heat of adsorption decreases to about 70 kJ mol⁻¹, showing that the interaction with the protons is less favorable than that with the sodium cations. In a neutron diffraction study of benzene in HY, Vitale et al.¹⁷ concluded that the benzene molecule in its adsorption site is facially coordinated to the H(2)

in the six-membered (6-T) ring, with a distance between the benzene center-of-mass (COM) and the proton of 3.40 Å. This was also concluded in HSAPO-37, both by IR spectroscopy¹⁸ and neutron diffraction.¹⁶ But the assignment is reportedly quite poor: based on similarities to what was observed in NaY the refinement was performed with the benzene molecule constrained next to an H(2) proton. The IR spectra of benzene sorbed in HY¹⁸ shows two components even at very low concentration, suggesting an interaction with two types of protons. Other very small bands were thought to belong to molecules adsorbed in the 12-T ring windows. A DFT study of benzene in interaction with an AlSi₂O₄H₉ cluster modeling an acid site of HY²¹ showed that the van der Waals (vdW) complex with a benzene molecule coordinated facially to the proton is the most stable complex, at an equilibrium H–COM distance of 3.22 Å. Note, however, that cluster Hartree–Fock calculations of the adsorption of benzene on acid sites in silica gel,⁴² that is, presenting terminal OH groups rather than bridging hydroxyls, led to two types of stable minimum energy sites: in the most stable site, benzene is coordinated to two protons on the same side, while in the second site, benzene is coordinated facially to only one proton. It has been also shown by multinuclear NMR experiments^{43,44} that for benzene the H-bond complex is more stable than the proton-transfer complex.

All these studies agree that the stable HY–benzene complex is of physisorbed type, that is, H-bond or vdW complex. This further justifies the present work, since it is likely that the diffusion process will be due to vdW interactions also. The exact nature of the adsorption site, however, is not so clear. It could not be completely determined from neutron diffraction data, most probably because of the large heterogeneity in the proton location, and hence in the adsorption sites. Cluster DFT and Hartree–Fock calculations suggest the existence of a stable complex involving the facial interaction of benzene with either one or two protons.²¹

Some studies also investigated the activation energy for the onset of mobility of benzene in HY. Sousa-Gonçalves et al.²⁰ used ²H NMR to measure an activation energy of less than 10 kJ mol⁻¹ at low temperature (210–260 K) and of approximately 25 kJ mol⁻¹ at higher temperature (260–292 K), assigned to the intracage and intercage mobilities, respectively. These energies are considerably lower than the activation energy reported for the mobility of the proton in HY in the presence of an adsorbed molecule:⁴⁵ 61 kJ mol⁻¹. Combined with the nonredistribution of the protons upon adsorption of benzene, this again justifies the neglect of chemical interaction.

In light of these data, we constructed a zeolite HY model with a ratio of Si/Al = 2.43. The initial atomic crystallographic positions were taken from the neutron diffraction data of Czjzek et al.³¹ The simulation cell consisted of a square box with $a = 24.77$ Å, with 136 Si, 56 Al, 384 O, and 56 H. The aluminum atoms were randomly distributed in the cell. 30 protons were placed at H(1), 10 at H(2), 16 at H(3), and 0 at H(4), using the following three rules: (i) protons are linked to an oxygen close to an Al atom; (ii) no two hydroxyl groups can be linked to the same silicon atom; (iii) no proton can be closer than 4.0 Å from another. Note that H(3) protons point inside the sodalite cages, and therefore have no importance as far as adsorption of benzene in the supercages is concerned. The only accessible protons are H(1) in the 4-T ring and H(2) in the 6-T ring. These rules do not determine completely the position of the protons. To investigate the influence of different proton distributions, three different initial configurations were prepared. Each structure was then minimized using MSI's Discover96 code with the force

field *cff91_zeo*.⁴⁶ Although the total energy of the structures differed by more than 400 kJ mol⁻¹ with this force field, it was found that all three final configurations were broadly equivalent as far as sorption of benzene is concerned. Indeed, the 40 accessible protons in any structure suffice to create a heterogeneity of the acidic sites larger than the difference between the structures. Therefore in what follows, only results for the most stable of these structures are given.

3. Computational Methods

3.1. Benzene—Faujasite Force Field. A wide class of force fields used to model adsorption in zeolites is referred to as the “average T-site” model, based on the approach of Kiselev and co-workers.⁴⁷ In these models, all tetrahedral atoms are considered to be equivalent and the negative charge due to the Al content is spread uniformly over all framework oxygen atoms. These force fields present the wonderful advantage of keeping perfect framework symmetry, irrespective of the Al content. Recently such types of force field have been shown to yield quantitative agreement for the heat of adsorption of chloroform in faujasite at any loading.^{48,49} Auerbach and co-workers used the same type of force field to study the adsorption and diffusion of benzene in NaX and also NaY showing good agreement with experiments at infinite dilution.^{3,5} But one can wonder if this symmetry introduced mainly to simplify the analysis of the simulation results does not hide artificially an underlying complexity. Indeed, to our knowledge no ordering of Al atoms in the framework has been found in faujasite with Si/Al > 1, which implies at the molecular level a heterogeneity of the cationic or acidic sites.³⁹ This heterogeneity prevails in protonated zeolites, where acidic hydroxyls are located next to Al sites. To study adsorption of benzene on HY, it is important to explore the effects from an “explicit Al” model and an according force field.

The explicit Al force field derived by Henson and co-workers^{32,50,51} based on the charges of Kramer and co-workers^{52,53} proved not to reproduce adequately the cation dynamics in faujasite,⁵⁴ which we feel comes from the overestimated difference of 1 |*e*| between the charges of Al and Si in their model. Indeed, this representation assumes a complete heterogeneity of the T-sites without any spreading of the excess charge on the O atoms, which is contradicted by most ab initio calculations of zeolitic charges,^{55,56} as well as electronegativity equilibration methods.^{57–59} These last methods show that atomic charges depend not only on nearest neighbors but also on next nearest neighbors and atoms even farther away. To place ourselves on the right middle ground between simplicity of the charge description and validity of the local environment, we chose to define different charges *q* for O atoms between two Si atoms (Oz), between an Si and an Al atom (Oa), and in a hydroxyl group (Ob), thus following the philosophy of the force field presented by Hill and Sauer.^{60,61} The derivation of our own parameters allows to compare more easily with previous calculations in sodium faujasite.^{3,5,7,8} Since this force field should be able to model NaX as well as NaY, dealuminated Y (DAY) or HY, the chosen charges should be conserved whatever the Si/Al ratio or the number of Na cations versus protons in the structure. Writing $\rho = n(\text{Si})/n(\text{Al})$ and $\gamma = n(\text{Na})/n(\text{H})$, the charge neutrality of the framework implies:

$$\rho q(\text{Si}) + q(\text{Al}) + \gamma q(\text{Na}) + (1 - \gamma)(q(\text{H}) + q(\text{Ob})) + (3 + \gamma)q(\text{Oa}) + 2(\rho - 1)q(\text{Oz}) = 0 \quad (1)$$

TABLE 1: Atomic Charges and Lennard-Jones Parameters Used to Model the Adsorption of Benzene in HY^a

element	charge	element	<i>A</i> /eV.Å ⁶	<i>B</i> /eV.Å ¹²
Si	+1.6 <i>e</i>	C–Oz	22.99	25 022.1
Al	+1.2 <i>e</i>	H–Oz	3.20	1563.1
Oz	–0.8 <i>e</i>	C–Oa	25.57	29 251.0
Oa	–0.9 <i>e</i>	H–Oa	3.71	1918.3
Ob	–0.3 <i>e</i>	C–Ob	18.63	18 331.7
H (zeolite)	+0.2 <i>e</i>	H–Ob	2.403	1045.9
C ^a	–0.153 <i>e</i>	C–Hz	2.588	1299.3
H (benzene) ^a	+0.153 <i>e</i>	H–Hz	0.455	88.1

^a See ref 3.

This relation should be verified for all ρ and γ , so that:

$$\left. \begin{aligned} q(\text{Si}) + 2 q(\text{Oz}) &= 0 \\ q(\text{Al}) + q(\text{Si}) + q(\text{Na}) + 4q(\text{Oa}) &= 0 \\ q(\text{Na}) + q(\text{Oa}) - q(\text{H}) - q(\text{Ob}) &= 0 \end{aligned} \right\} \quad (2)$$

The above set of equations of course does not completely determine the charges and several other assumptions have to be made. Based on ab initio calculations on clusters^{55,56,62} and periodic Hartree–Fock calculations⁶³ as well as experimental measurements of the phonon modes⁵⁵ or fitting of the X-ray electron density map,⁶⁴ we chose the atomic charge values listed in Table 1. The magnitude of the charges in this set is significantly lower than the Kramer-based charges.⁵³ However, except for the Al atom, they are rather close to the atomic charges fitted to DFT calculations recently published by Blake et al.⁶⁵

The benzene–zeolite interactions are modeled using a simple 6–12–1 potential between each guest–zeolite atom pair:

$$U = \sum_{iJ} \left(-\frac{A_{iJ}}{r_{iJ}^6} + \frac{B_{iJ}}{r_{iJ}^{12}} + \frac{q_i q_J}{r_{iJ}} \right) \quad (3)$$

i and *J* referring to the guest and zeolite atoms, respectively, and using for the Coulombic part the charges defined above. The coefficients *A*_{*ij*} and *B*_{*ij*} of the potential were assigned by comparison of adsorption and diffusion simulations to experimental data for NaX, NaY, DAY, and HY. A combination rule based on Slater–Kirkwood’s expression of the dispersion force⁶⁶ was used to relate atomic parameters to the Lennard-Jones coefficients. All relevant parameters are listed in Table 1. In all calculations the zeolite framework was held fixed. The internal potential function for benzene, as well as the benzene–benzene interactions, are the same as in ref 3. Short-range interactions were cut off at 12.0 Å, while long-range electrostatic energies and forces were computed either with an Ewald procedure optimized for the simulation of flexible guest molecules sorbed within a rigid host, or with the fast multipole method^{67,68} as implemented in ref 7. All calculations involving host–guest interactions were performed using the DIZZY code developed by Henson and subsequently modified in-house by Auerbach and co-workers.^{7,69}

3.2. Theory of Rate Constant Calculations. The rate constant for a jump from an initial site *i* to a final site *j* can be expressed within flux correlation theory as:^{70,71}

$$k_{i \rightarrow j}(t) = \frac{1}{\chi_i} \langle \dot{z}(0) \delta_i[\mathbf{r}(0)] \Theta_j[\mathbf{r}(t)] \rangle \quad (4)$$

where χ_i is the equilibrium mole fraction of particles in the state *i*, *z* the coordinate perpendicular to the dividing surface bounding state *i*, \dot{z} its time derivative, $\delta_i[\mathbf{r}]$ the Dirac delta function

$\delta[\mathbf{r}-\mathbf{r}_i^\ddagger]$ with \mathbf{r}_i^\ddagger representing the boundary of state i , and $\Theta_j[\mathbf{r}]$ the standard step function whose value is 1 if the particle is in state j and zero otherwise.

This equation represents the flux of particles through the boundary surface of state i at time $t = 0$ that are found in state j at time t . If a particle “thermalizes” in the final state j , that is, if it loses the translational energy that allows the diffusion of matter from site to site, $k_{i \rightarrow j}(t)$ will tend to a plateau after a certain time.⁷¹ For benzene in NaY at 300 K, the plateau was found to be reached after $t \approx 3$ ps.⁷ This value determines the microscopically exact rate constant to be used in kinetic Monte Carlo (KMC) simulations of diffusion in zeolites.¹³ It has the property that it does not depend, in theory, on the choice of the boundary surface of the states, although the accuracy of the calculation is strongly dependent.

The transition state theory (TST) rate constant between two neighboring sites i and j can be written using the same kind of notation:

$$k_{i \rightarrow j}^{\text{TST}} = \frac{1}{\chi_i} \langle \dot{z}(0) \delta_i[\mathbf{r}(0)] \Theta_j[\mathbf{r}(\epsilon)] \rangle \quad (5)$$

where ϵ now represents a very short time: all trajectories leaving site i at $t = 0$ in the direction of site j will by definition be found in site j just afterward. As a consequence, half of all trajectories are considered reactive, and eq 5 is strongly dependent on the choice of the transition state. The rate constant can be rewritten in the usual form:

$$k_{i \rightarrow j}^{\text{TST}} = \frac{1}{2} \left(\frac{2k_B T}{\pi m} \right)^{1/2} \frac{Q^\ddagger}{Q_i} \quad (6)$$

where Q^\ddagger is the configurational partition function at the transition state, Q_i the one in the reactant state i , k_B being Boltzmann constant, T the temperature, and m the particle mass.⁷² The last expression can be calculated from a Monte Carlo calculation and allows us to write the exact rate constant as:

$$k_{i \rightarrow j}(t) = k_{i \rightarrow j}^{\text{TST}} \times f_{ij}(t) \quad (7)$$

wherein we have defined the so-called dynamic correction factor as:

$$f_{ij}(t) = \frac{\langle \dot{z}(0) \delta_i[\mathbf{r}(0)] \Theta_j[\mathbf{r}(t)] \rangle}{\langle \dot{z}(0) \delta_i[\mathbf{r}(0)] \Theta_j[\mathbf{r}(\epsilon)] \rangle} \quad (8)$$

This factor in turn can be calculated using short nonequilibrium molecular dynamics simulations, initialized at the transition state. As can be seen from the theory, several steps are required to finally attain the microscopically exact rate constants: (i) the sites, as well as their boundaries, should be defined and characterized; (ii) the TST rate constants between the sites need to be evaluated; (iii) nonequilibrium molecular dynamics runs allow the calculation of the flux correlation rates.

3.3. Simulation Procedures. A variety of force field based computational techniques were used to model the adsorption of benzene in HY, namely: (i) molecular docking to find the minimum energy sites of the sorbed molecules; (ii) equilibrium molecular dynamics (MD) at room temperature to investigate the stability of the sites and the external motions of the sorbed molecule; (iii) constrained minimization to find out the minimum energy path (MEP) between some of the stable sites; (iv) Monte Carlo (MC) umbrella sampling to investigate the temperature dependence of the transition state theory (TST) hopping

probabilities; and (v) nonequilibrium MD for the calculation of the dynamic corrections to the rate constants.

The docking procedure used in this study is described in ref 3. A single molecule is put in the zeolite framework and given a random translational “kick,” followed by 1000 steps of high-temperature MD, with a 1 fs time step; this starting structure is then minimized. 300 initial configurations were analyzed. The minimization procedure locates minimum energy sites, that is, stable adsorption sites at 0 K. However, there is no guarantee that *all* sites in the simulation cell are found. Furthermore, the sites may be bound by very low energy barriers, and therefore be unstable sites even at very low temperature. Therefore in each distinct site located by the docking procedure we run a 20 ps MD at 200 K to determine if it is a stable adsorption site at this temperature. If so the distance distribution with the closest protons was calculated from the MD results. The low-frequency vibrational density of states (VDOS) of the sorbed benzene was also calculated from the center of mass (COM) velocity autocorrelation function in order to characterize the external benzene motions at each stable site.^{7,73,74}

$$\text{VDOS}(\sigma) = \int dt \exp(-i2\pi c\sigma t) \frac{\langle \mathbf{v}(t) \cdot \mathbf{v}(0) \rangle}{\langle \mathbf{v}(0) \cdot \mathbf{v}(0) \rangle} \quad (9)$$

where c is the speed of light, σ the wavenumber counted in cm^{-1} , and \mathbf{v} the COM velocity. We should point out that since protons are fixed during the simulation we cannot observe the coupling between the hydroxyl vibrations and those of benzene. We have shown that in the case of NaY, the coupling between the cation and benzene can change the observed vibrational frequency by a factor of ca. 2.⁷⁵ Thus we should consider the peaks in the VDOS only as indicative of the benzene COM motions in the different sites and not as quantitatively comparable to experiment.

The constrained minimization procedure of ref 3 was then applied to determine the MEP between the sites: at each step along a path going from one site to another the benzene molecular COM is constrained to stay in a plane perpendicular to the path, and its position in the plane and internal degrees of freedom are minimized. Note that this supposes that the reaction coordinate is isomorphous to the position of the molecular COM, which is reasonable since we are interested in the transport of matter inside the zeolite. We focused on determining the mechanism of the cage-to-cage motion of benzene in HY by looking at a path beginning at a stable site in one supercage and ending in another cage.

The TST rate constant calculated by eq 6 mainly depends on the ratio Q^\ddagger/Q_i , which can be related to a kind of potential of mean force $F(z)$ ⁷⁶ by defining a restricted partition function:

$$Q(z) = \int dz' \delta(z - z') \int d\mathbf{r}^N \exp(-\beta E[z', \mathbf{r}^N]) = \exp - \beta F(z) \quad (10)$$

where $E[z', \mathbf{r}^N]$ is the energy of the configuration defined by \mathbf{r}^N , so that the rate constant becomes:

$$k_{i \rightarrow j}^{\text{TST}} = \frac{1}{2} \left(\frac{2k_B T}{\pi m} \right)^{1/2} \frac{\exp - \beta F(z^\ddagger)}{\int_i \exp - \beta F(z) dz} \quad (11)$$

Computing the TST rates is therefore equivalent to calculate free energy differences. Numerous methods have been developed over the years,^{76,77} and it is still an area of active research.^{78–83} In a previous publication about benzene in NaY⁷ we used the displacement vector method of Voter,⁸⁴ which

presents the advantage of requiring only two constrained MC calculations, one in the initial state and one in the final state. In the case of HY however, some difficulties arise due to the heterogeneous distribution of the protons, so that the adsorption sites are not symmetrical and well-defined paths leading from one single site to another no longer exist. We chose instead the simple implementation of the umbrella sampling method⁸⁵ presented in ref 76 as “self-consistent histogram window sampling” (SCHWS).

The reaction path determined by constrained minimization is cut into smaller slices, overlapping on one-third of their length with the next interval. In each interval we calculate the probability distribution (PD):

$$p_i(z) = \frac{\exp - \beta F(z)}{\int_{z_i^{\min}}^{z_i^{\max}} dz' \exp - \beta F(z')} \quad (12)$$

The complete distribution is then reconstructed from the PD in each interval using the procedure indicated in ref 76. A plot of $F(z) = -k_B T \ln p(z)$ can be interpreted as the constrained free energy profile along the reaction coordinate z . For a perfectly entropy-free, energy-driven reaction this plot would not display any temperature dependence, indicating an Arrhenius dependence for the rates; thus any temperature dependence can be related to the entropy change during the reaction.

Depending on the MEP investigated, a 8 to 9 Å path was cut into 15 slices, thus building 0.8 to 1.0 Å intervals. The PD in each slice was calculated from 10^5 MC steps at 200, 300, 400, and 600 K. From the resulting profile we used two approximations of Q_i to compute the TST rate constant: (i) from direct integration of $p(z)$ over the “initial state” basins; (ii) from a fit of $F(z) = -k_B T \ln p(z)$ around the bottom of the free energy well by a quadratic function $F^*(z) = F_0 + k(z - z_0)^2$, followed by integration over the fitted well:

$$k^{\text{TST}} = \frac{1}{2} \left(\frac{2k_B T}{\pi m} \right)^{1/2} \exp - \beta (F(z^\ddagger) - F_0) \quad (13)$$

The purpose of these two calculations is to estimate the order of magnitude of the uncertainty on k^{TST} by approximating $\Delta k^{\text{TST}} \approx |k_1^{\text{TST}} - k_2^{\text{TST}}|$.

In contrast to what was found in NaY,⁷ several different minimum energy sites can be found for similar values of the reaction coordinate; a converged MC at high temperature will therefore sample all these sites. Although this is perfectly fine for adsorption studies, we need to be somewhat more cautious since we are interested in the dynamics of the sorbed molecule: indeed, our sampling should not allow the molecule to cross unrealistically high energy barriers at a given temperature. The maximum size of the MC steps was therefore limited to ~ 0.3 Å. The corresponding acceptance rate varied between 0.4 and 0.7, depending on temperature. Despite this restriction, we observed during the MC runs “multi-site” sampling. We have verified that in most cases longer sampling improved the statistical accuracy but did not change the calculated average probabilities. Thus, the multisite sampling physically means that at this temperature one average site exists encompassing multiple 0 K adsorption sites. An exception will be discussed in Section 4.

Following variational TST, transition states on the diffusion path can be defined as the positions for which the probability of presence is minimum. Dynamic corrections were computed as the average over 2000 short nonequilibrium MD runs initialized from a MC sampling constrained at this transition

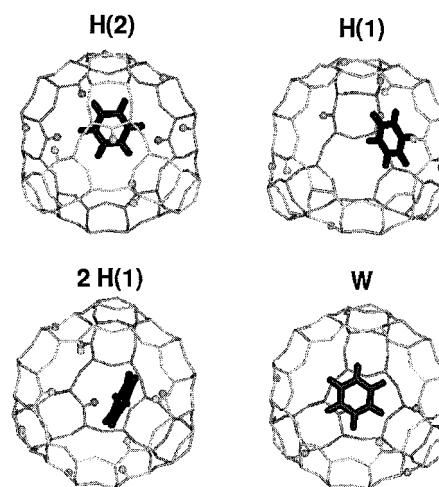


Figure 1. Examples of the four classes of minimum energy position of benzene in the zeolite HY model with Si/Al = 2.43, as determined with the docking procedure using the DIZZY code with the in-house force field detailed in the text. White balls represent zeolite protons.

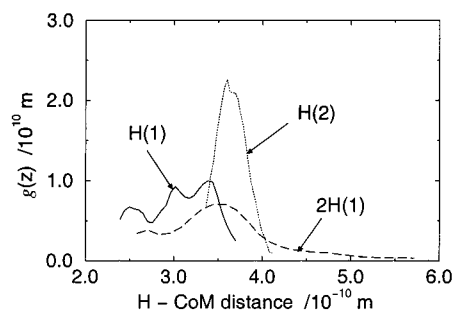


Figure 2. Probability density distribution of the zeolite H(n)-benzene COM distance. Each curve is calculated from the average over a 20 ps MD run at 200 K with a 1 fs time step in all distinct and stable sites of the same class; results obtained using the DIZZY code with the in-house force field indicated in the text.

state, with initial velocities assigned from a Maxwell-Boltzmann distribution at the required temperature. All trajectories were run for 5 ps, with a 1 fs time step. We computed the dynamic factor correcting the TST rate constants for the probability to find the guest molecule at a particular site, and also for the probability to find the molecule left and right of the transition state. The uncertainty of $f(t)$ is estimated as the 95% confidence interval on the average value. From eq 8 we see that the total uncertainty on k is $\Delta k/k = \Delta k^{\text{TST}}/k^{\text{TST}} + \Delta f/f$.

4. Results and Discussion

4.1. Adsorption Sites. From the molecular docking of 300 initial benzene structures inside our HY model, we obtained 46 different minimized configurations; among these structures, only 30 remained stable during a 20 ps MD run at 200 K, while all others moved to another cataloged minimum energy position. Based on the local geometry of the site, they can be categorized in four classes, noted H(1), H(2), 2H(1), and W. One example minimum energy configuration of each of the four classes is depicted in Figure 1. Figure 2 presents the relevant probability density distribution of the zeolite proton-benzene COM distance for each class (except W) calculated from the average over all distinct sites in the class obtained by a 20 ps MD trajectory at 200 K, while Figure 3 presents the averaged low-frequency vibrational density of states (VDOS) of the benzene COM in all classes.

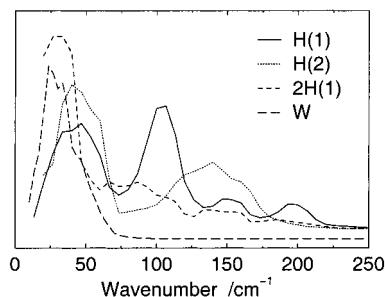


Figure 3. Low-frequency vibrational density of states of the benzene center of mass. Each curve is calculated from the average over a 20 ps MD run at 200 K with a 1 fs time step in all distinct and stable sites of the same class; results obtained using the DIZZY code with the in-house force field indicated in the text.

4.1.1. H(1). The benzene molecule is facially coordinated to a H(1) proton in a 12-T ring window, with an interaction energy at 0 K varying between -58.8 and -45.3 kJ mol $^{-1}$. The distance between the benzene COM and the zeolite proton in the minimized configuration varies between 2.4 and 3.3 Å, depending on the environment. There is no clear correlation between this distance and the interaction energy. The dynamic distribution of distances at 200 K presents three distinct peaks at 2.5, 3.0, and 3.4 Å, showing a rather tight binding between the proton and adsorbed benzene. This is confirmed by the VDOS in site H(1) which presents several peaks at quite high frequencies for adsorbed molecules, that is, 150 and 200 cm $^{-1}$, corresponding to the H–COM stretching. The presence of two peaks at lower frequencies shows the existence of other types of translational motions parallel to the zeolite wall.

4.1.2. H(2). The benzene molecule is facially coordinated to a H(2) proton in a 6-T ring, with an interaction energy varying between -56.8 and -39.0 kJ mol $^{-1}$. The H(2)–COM distance is in general larger than for H(1): $3.4 < d(\text{H}(2)\text{--COM}) < 4.0$ Å, because the H(2) proton protrudes much less from the O frame than the H(1). A large part of the interaction stems therefore from zeolite oxygen–benzene hydrogen interaction. As a consequence, a slight correlation is found between the number of Oa versus Oz atoms closest to the benzene hydrogens and the interaction energy: the more Oa's the larger the magnitude of the interaction. Several other factors may however play a role, most notably the presence or absence of a H(1) proton nearby. The dynamic distribution of distances also shows a single narrow peak at 3.6 Å, close to the distance of 3.4 Å deduced from neutron diffraction by Vitale et al.¹⁷ On the VDOS a single broad high-frequency peak around 150 cm $^{-1}$ shows that the H(2)–COM stretching is generally less tight than that for H(1)–COM. The translational motions at lower frequencies, on the other hand, show no difference with H(1).

4.1.3. 2H(1). The benzene molecule is facially coordinated to two H(1) protons, either in the same 12-T ring or in the same 4-T ring. The distance between the two protons amounts to about 4 Å. The interaction energy varies between -56.7 and -44.1 kJ mol $^{-1}$, that is, nearly identical to what was found for 1H(1). The benzene 2H(1)–COM distances at 0 K varies between 2.7 and ~ 4.5 Å; once again there is no correlation between the zeolite O and benzene H distance and the interaction energy. During the MD simulation, we found that a molecule at a 2H(1) site could shift between a position where it lies closer to one proton or the other. This suggests the existence of rather low energy barriers between these equivalent positions; it creates a long “supersite” next to the protonated groups, materialized by the long tail observed for the 2H(1)–COM distribution in Figure 2. Since benzene is not linked to a single proton, no well-defined

high-frequency stretching peak is observed on the VDOS, but rather a long tail decaying at ~ 200 cm $^{-1}$. The low-frequency component of the spectrum peaked at even lower frequencies than those of H(1) and H(2), showing that the translational parallel motion in this longer supersite is less constrained. As described in Section 2, no special care was taken to maximize the distance between zeolite protons during the protonation procedure, as long as they were more than 4 Å apart. Thus the number of such double hydroxyl groups might be overestimated as compared to experimental structures.

4.1.4. W. W stands for a “window” site similar to what is found in NaY: the benzene molecule is framed by the 12-T window and stabilized by zeolite O–benzene H interactions. Only one such stable site at 200 K was found, with an interaction energy of -41.9 kJ mol $^{-1}$. The involved window is not a particularly Al rich one, since it contains 4 Al and 8 Si atoms, the average being 3.5 Al and 8.5 Si. Although this site remains stable during the dynamics, its relatively high energy places it among the less probable adsorption sites. This is corroborated by its single occurrence among the stable sites. The VDOS in this site shows a single component at very low frequency, in accordance with what was observed in NaY for the same site.⁷

Neutron diffraction experiments¹⁷ that located the H(2) sites did not report the existence of a benzene site next to a H(1), which we predict are the most stable sites. This might come from the low symmetry of the H(1) protons in the zeolite cage, as well as the existence of two adsorption sites involving these protons: H(1) and 2H(1). Quantum mechanical calculations^{21,42} as well as infrared studies,^{18,19} however, suggest the existence of such sites. A novelty here is the presence of 2H(1) sites, that were theoretically postulated in silica gels⁴² but, to our knowledge, never reported for Brønsted acid sites in zeolites. All parameter sets we tried, however, lead to sites of this type when two H(1) protons are sufficiently close. Note that we also constructed a first zeolite model in which we allowed possible Al–OH–Si–OH–Al groups; in this model and with the same force field we could find close H(1) and H(2) protons that also induced an adsorption site for benzene similar to 2H(1); the influence of the protons therefore predominates over that of the rest of the framework. The finding of a less stabilized W site also agrees with IR measurements of very small bands thought to belong to benzene molecules in the 12-T rings.^{18,19} The clear picture resulting from our calculations is that of a facially coordinated van der Waals complex between hydroxyl groups at H(1) or H(2) and the benzene molecule. The interaction energies do not seem to depend directly on the local geometry of this complex, but rather on the distribution of aluminum, protons, and Oa and Oz types of oxygen in the vicinity. It induces a large heterogeneity of the interaction energies, amounting to 20 kJ mol $^{-1}$. Some sites were found over unprotonated 4- and 6-T rings, similar to what has been observed in dealuminated Y;^{32,51,86} these high energy sites, however, did not appear to be stable during the short 200 K MD runs.

4.2. Site-to-Site Dynamics. **4.2.1. Minimum Energy Paths.** The docking procedure presented in the previous section located multiple sites for benzene adsorption in HY, with a large heterogeneity of host–guest interaction energies. There is no a priori way to determine if a molecule can go from one site to any other without relaxing somewhere in between; the possible pathways are therefore too numerous to be studied extensively, and we need to focus on some selected ones. We chose to study a pathway starting at a 2H(1) site in a cage, crossing a window, and ending at a H(1) site in a neighboring cage. This path was chosen arbitrarily to sample most site types (a H(2) proton being

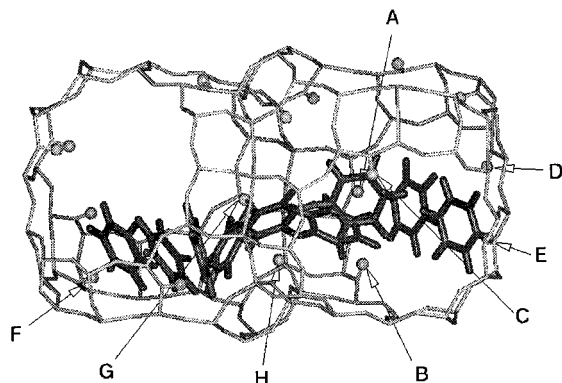


Figure 4. View of the successive positions of benzene along one minimum energy path between two cages of HY, as calculated by the constrained minimization procedure indicated in the text. White balls represent zeolite protons. All results were obtained using the DIZZY code with the in-house force field indicated in the text.

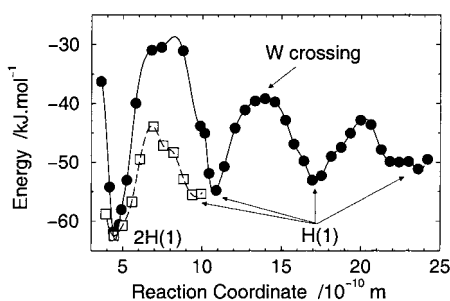


Figure 5. Energy profiles of selected minimum energy paths of benzene in HY, as calculated by the constrained minimization procedure using the DIZZY code with the in-house force field indicated in the text. Circles: path corresponding to Figure 4; squares: alternative path going out of the same initial 2H(1) site. Lines are splines of the calculated points.

close to the path), but no attention was paid to the energy of the particular sites encountered along the path. Most probably, another choice of pathways would lead to numerically different results. We are confident, however, that the conclusions drawn from the analyses would remain unchanged.

Figure 4 presents the minimum energy pathway (MEP) calculated from successive constrained energy minimizations in a plane along a path from one far end of a cage to the far end of the next; the corresponding energy profile is presented in Figure 5. For convenience, we have labeled some of the protons accessible to adsorbed benzene from A to H. The molecule starts at a very deep 2H(1) site (F), goes through a “cartwheel” jump to a H(1) site on the side of the 12-T window (H), glides over the wall of the window to end next to the same H(1) proton but on the other side of the window (H), and reorients toward another H(1) opening in another window (A). The 2H(1) \rightarrow H(1) jump proceeds with a high energy barrier of more than 30 kJ mol⁻¹, while the “gliding” jumps present smaller barriers of \sim 20 kJ mol⁻¹. There are two reasons for this high difference: first, the 2H(1) site investigated here is fortuitously deeper than the other sites; and second, the chosen path constrains the benzene to move away from the proton toward the center of a cage, which is very generally a high energy site for small molecules,⁸⁷ while in the other cases benzene remains parallel to the wall. Indeed, in Figure 5 the MEP is also presented leading out of the same 2H(1) site (F) toward a H(1) site with the benzene molecule parallel to the wall; this path proceeds via a gliding motion with an energy barrier of 20 kJ mol⁻¹. It is therefore likely that the cartwheel jump evidenced by our simulation would not play any significant

role in benzene diffusion at low temperatures. The window crossing mechanism is completely different to what has been postulated in NaX and NaY.¹³ Indeed, the benzene molecule glides from a H(1) site on one side of the window to the other side, in a sort of proton-assisted jump. Most probably, consideration of the framework motions and especially of those of the protons will reduce this already low energy barrier, by allowing the host protons to follow the guest molecule. The 20 kJ mol⁻¹ barrier observed for this motion makes the conventional cage-to-cage jump through a W site relatively unlikely, since the energy of the latter stable site is equal to that of the maximum of the barrier.

The calculated energy barriers are close to the ones measured at high temperatures by ²H NMR:²⁰ 25 kJ mol⁻¹. We also obtain low energy barriers that could correlate with the 10 kJ mol⁻¹ energy barrier found by the same group at low temperature. It seems that gliding along the walls between H(1), H(2), and 2H(1) sites constitutes the lowest energy pathways for benzene diffusion in HY. The window crossing mechanism does not appear to be any different from other site-to-site motions, and has a rather low energy profile. At low temperatures, mass transport through HY therefore appears as though proceeding through creeping along the walls between nearby H(1), H(2), and 2H(1) sites, with energy barriers of approximately 15–20 kJ mol⁻¹. Since the accessible protons are rather numerous in the HY zeolite model (Si/Al = 2.43) we are using, there should not be any trapping of benzene at a position from which it cannot move through this same creeping mechanism; in particular, the probability that a window does not present any H(1) proton is small so that the probability that all four windows in a cage are protonless is tiny. As the Si/Al ratio increases, the number of protons decreases and we would expect more and more trapping sites. As a consequence we expect the energy barrier for benzene transport to increase. Indeed, Sousa-Gonçalves et al.²⁰ report for benzene in dealuminated Y an activation energy at high temperature of 30 kJ mol⁻¹, larger than in HY. Note however that Bull et al.³² only report an activation energy of 10.2 kJ mol⁻¹ in dealuminated Y.

4.2.2. Temperature Dependence of the Diffusion Path. The diffusion path studied presents three distinct jumps, that is, intracage 2H(1) \rightarrow H(1) via cartwheel motion, intercage H(1) \rightarrow H(1) via a smooth glide over the window, and intracage H(1) \rightarrow H(1) via reorientation. To study the influence of temperature using self-consistent histogram window sampling (SCHWS) we chose to cut the previous path in three distinct parts, each starting at the minimum energy position in one of the site and ending at the minimum energy position in the other. The three paths were then smoothly merged at the minimum energy positions. As a consequence the constrained reaction coordinate is slightly modified as compared to Figure 5. Results of the SCHWS are presented in Figure 6, together with the minimum energy path (MEP) already presented in Figure 5. A notable temperature dependence of the plots indicates a strong influence of the entropy on the molecular motions. The curves look quite different from the MEP. First, the energy of the minima seems to be very largely shifted toward higher energy as compared to the deepest minimum, that is, the initial 2H(1) site. In fact this effect is an artifact of the calculation, due to the very low stability of the 2H(1) \rightarrow H(1) cartwheel jump. Indeed, the MC runs in the initial slices sample paths where benzene glides along the wall to another H(1) site; after several intervals these paths are no longer accessible, and the MC runs then sample another path next to the H(1) proton. This introduces a discontinuity in the sampling, shown by the apparent shift in Figure 6. In the

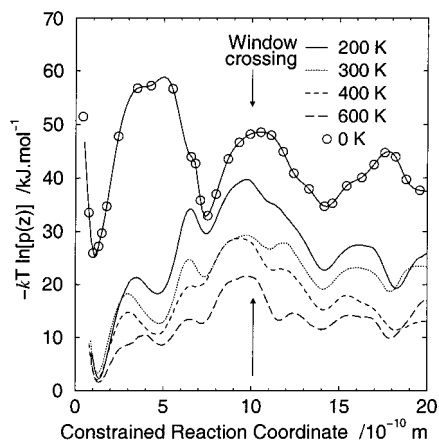


Figure 6. Constrained free energy profile $F(z) = k_B T \ln[p(z)]$ of benzene in zeolite HY, calculated using the SCHWS procedure and the DIZZY code with the in-house force field indicated in the text. The curves were translated so that the first minimum at ~ 1 Å has the same energy at all temperatures. Circles: results of the constrained minimization calculation presented in Figure 5; for readability, this curve was translated upward from the free energy curves.

following discussion, we will therefore neglect the 2H(1) site. Second, other minima appear around 5, 11, and 18 Å. The minimum at 5 Å corresponds to the sampling of a H(2) \rightarrow H(1) path instead of the 2H(1) \rightarrow H(1) path, as discussed above. The minimum at 11 Å, on the other hand, becomes more and more apparent as the temperature increases; this comes from the availability of another H(1) proton located at about 7.5 Å on the other side of the window, both sites being sampled at the same time. The “hollowing” with increasing temperature can be interpreted in the following way: at low temperatures, the most probable path from the H(1) site in one cage to the next cage will be by the gliding motion presented in Figure 4, which indeed is the only one accessible at 0 K; when the temperature increases, another path is sampled, namely a jump across the window to another H(1) proton, then from this new H(1) to the final H(1) site on the other side of the original proton, or alternatively to another proton in the cage. Both paths exist at the temperatures studied. When benzene leaves the window by the other H(1) proton other pathways for diffusion in the final cage become available: these are the reasons for the appearance of another minimum at ~ 18 Å.

4.2.3. Rate Constants. The existence of multiple pathways for benzene diffusing in zeolite HY complicates the interpretation of the self-consistent histogram window sampling (SCHWS) results. Since even at low temperature (200 K) distinct sites at 0 K are merged into larger supersites sampled by the Monte Carlo (MC) runs, we cannot give a simple interpretation of site-to-site rate constants to the probabilities extracted from Figure 6. Mass transport in HY however implies that benzene molecules go from one cage to another through a window. We will therefore focus on calculating the rates for the window crossing, with transition state theory (TST) from eq 6, and with flux correlation theory (CF). As indicated before, several different sites can coexist on each side of the transition state. In this context, it is not always meaningful to compute a site-to-site rate constant. However, TST rates are simply defined as the flux of molecules crossing the transition state to the left and to the right; a meaningful dynamic correction factor then is the probability to find the molecule left or right of the transition state after a certain time. We also defined molecules to be in individual “sites” when the benzene COM is less than 4 Å from a proton. These sites are not exactly equivalent to the 0 K adsorption sites defined in Section 4.1. However, they provide

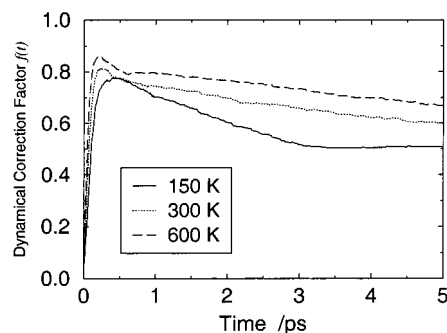


Figure 7. Dynamic correction factor $f(t)$ for the window crossing mechanism of benzene in zeolite HY. All curves are the average over 2000 nonequilibrium molecular dynamics trajectories, using the DIZZY code with the in-house force field indicated in the text.

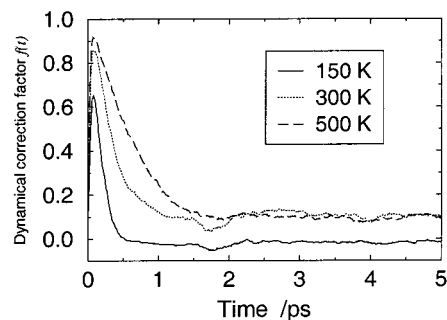


Figure 8. Dynamic correction factor $f(t)$ for the 2H(1) \rightarrow H(1) intracage jump, with the molecule initially positioned at 6.5 Å in Figure 6, calculated as the average over 2000 nonequilibrium molecular dynamics trajectories using the DIZZY code and the in-house force field presented in the text.

a useful measure of the zeolite proton–benzene attraction. In addition to the temperatures between 200 and 600 K already studied for the whole path, we computed the TST and CF rates for 150 and 800 K.

Figure 7 presents the dynamic correction factor $f(t)$ for the window crossing at three temperatures. Each curve is the average of over ~ 2000 nonequilibrium molecular dynamics (MD) trajectories initialized from a MC run constrained around 10 Å along the modified reaction coordinate in Figure 6, and lasted for 5 ps with a 1 fs time step. The initial rise of $f(t)$ is an artifact of the calculation, due to the fact that the transition state (TS) on which the MC run is performed has a certain width, for practical purposes. The rapid initial decrease of $f(t)$ is followed not exactly by a plateau but by a gently decreasing slope. As indicated in ref 22, the plateau value represents in fact an exponential decrease of $f(t)$, whose rate should be the rate constant; therefore, the dynamic correction to be used is the limiting value of this slope toward $t = 0$.

As can be seen in Figure 7, the correction factor is only weakly temperature dependent, decreasing from ~ 0.8 at 600 K to ~ 0.5 at 150 K; the resulting effect therefore is to decrease the activation energy for the window crossing, but only slightly. The correction factor is rather high: up to 0.8, showing that the choice of a reaction coordinate and of the TS is meaningful: a good percentage of the trajectories crossing the window to the left (or to the right, respectively) will be found at any time $t < 5$ ps later on the left cage (or the right cage, respectively). This is in contrast to what is observed for intracage motions, such as the 2H(1) \rightarrow H(1) with TS at 6.5 Å in Figure 6. Indeed, the corresponding dynamic correction factor displayed in Figure 8 for three temperatures presents a very rapid initial decrease, reaching zero in less than 0.5 ps for 150 K. This means that there is as much probability to find the molecule to the left

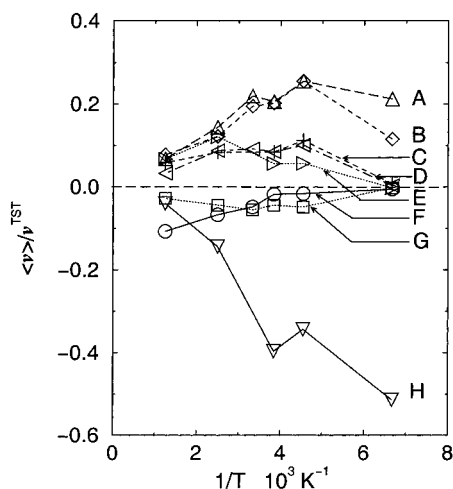


Figure 9. Proportion of the nonequilibrium MD runs ending in a particular site $\alpha = A, B, \dots G$ indicated in Figure 4.

or the right of the assumed TS after 0.5 ps whatever its original direction. Since the chosen TS is a maximum of constrained free energy it has a physical meaning as a position of low probability to find the molecule. Therefore, the decrease to zero means that the molecule does not relax in any of the sites to the left or the right of the TS even at this low temperature.

Figure 9 presents in more detail the sites in which the benzene molecules are found at the end of the 5 ps nonequilibrium MD runs. More precisely, the ordinate counts $\langle \nu_\alpha \rangle / \nu^{\text{TST}}$, where $\langle \nu_\alpha \rangle = 1/N \sum_{i=1}^N \mathbf{v}_i(0) \cdot \mathbf{n} \delta_i^\alpha(5 \text{ ps})$ is the average velocity of the MD runs that end after 5 ps in site α . ν^{TST} being a positive quantity, the positive values of $\langle \nu_\alpha \rangle$ indicate that the molecule ends on the right-hand side of the window, and the negative value on the left-hand side. The site labels correspond to Figure 4. We do not require here that the molecule relax in the site, but only that it is found in it at the end of the 5 ps MD run. Note also that, to simplify the figures, not all sites are indicated. At 150 K, most of the MD runs end next to the three protons labeled H, A, and B. These sites correspond to the original H(1) site on the left-hand side of the window in Figure 4, and two H(1) sites on the other side of the window. This is in agreement with the finding that at this low temperature the SCHWS procedure only samples the sites close to the minimum energy path (MEP). As the temperature increases, a number of other sites are populated. However, up to 400 K the same three protons close to the MEP remain the most attractive sites. The two A and B protons are close to each other, so that above 150 K they build a unique supersite which is shown by the coincidence of the A and B curves in Figure 9. Above 400 K, all protons become roughly equivalent.

Figure 10 presents the TST rate constants calculated for the window crossing mechanism, both by direct integration and using eq 13, as well as the dynamically corrected rates k^{CF} . The corresponding activation energies are summarized in Table 2. The rate constant from the left cage to the right cage k_{lr} presents a global Arrhenius dependence with temperature, with an activation energy of about 13.2 kJ mol^{-1} . Although the rate constant for a jump from the right cage to the left cage k_{rl} decreases with increasing inverse temperature, its dependence is not strictly linear. We can define roughly three temperature domains: (i) below 200 K, (ii) between 200 and 300 K, and (iii) above 300 K. At high temperature, the activation energy, 13.8 kJ mol^{-1} , is very close to that of k_{lr} . In the middle temperature range, the apparent activation energy is much higher: 32.8 kJ mol^{-1} . Finally at low temperature the activation

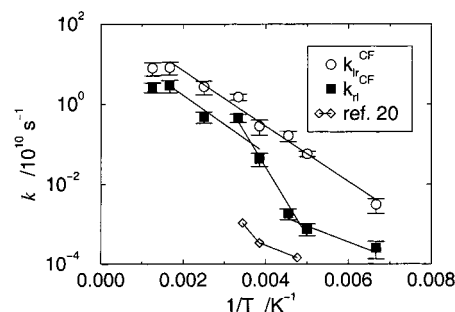


Figure 10. Correlation function rate constants for the window crossing, from left to right k_{lr} and from right to left k_{rl} calculated by eqs 6, 8, and 13. The lines indicate the mobility factor calculated from NMR data by Sousa-Gonçalves et al.²⁰

TABLE 2: Activation Energies for the Window Crossing of Benzene in Zeolite HY from Correlation Function Rate Constants Presented in Figure 10^a

rate	temperature range (K)	value (kJ mol ⁻¹)
k_{lr}	150–600 K	13.2 ± 0.8
k_{rl}	150–220 K	7.6 ± 1.7
k_{rl}	200–300 K	32.8 ± 3.1
k_{rl}	260–600 K	13.8 ± 4.1
k_{exp}^b	210–260 K	10
k_{exp}^b	260–292 K	25

^a k_{lr} is the rate constant for a window crossing from the cage on the left of Figure 4, to the cage on the right of Figure 4, k_{rl} the rate of the window crossing from the right cage to the left cage. ^b See ref 20.

energy of k_{rl} decreases to only 7.6 kJ mol^{-1} . The reason for the different behavior of k_{rl} as compared to k_{lr} can be found in Figure 6. Indeed the potential of mean force on the left-hand side of the window presents the same profile, whatever the temperature. On the right-hand side however, as indicated in Section 4.2.2., the profile changes as the temperature increases, reflecting the opening of different pathways out of the window. The activation energies we estimated are quite close to the experimental data of Sousa-Gonçalves et al.²⁰ which also present a change around 260 K. While they attributed this change to intracage and intercage mobility, our results suggest that it could be due to multiple crossing pathways for the same type of cage-to-cage motions. The large differences in activation energies, depending on the pathway and on the temperature, indicate a large heterogeneity of the rate constants. The influence of this heterogeneity is rather difficult to quantify exactly. Indeed, if we suppose that these activation energies are Gaussian distributed around E_0 with a variance σ^2 , we have that:¹³ $\langle k \rangle \approx \nu \exp(-\beta E_0) \exp(-\beta^2 \sigma^2 / 2)$; that is, the apparent average activation energy deduced from measures of the rates will appear somewhat *larger* than the average activation energy, especially at low temperatures. This comes from the trapping of the molecules in sites with high activation energies.

5. Conclusion

The theoretical simulations relative to the adsorption and diffusion of benzene in zeolite HY presented in this article lead to a number of conclusions that can help to interpret some experimental data on this widely used system. Like all other force field based simulations, the numerical results we obtain depend on the potential used. We parametrized a new force field on experimental data for benzene adsorption and diffusion in different zeolites of faujasite type. Through this parametrization we gained some insight into the influence of the parameters, and we are confident that the philosophy of our results would

remain the same for any force field using related charges and potential energy functions.

Molecular docking and minimization have shown that in the most important minimum energy sites benzene is coordinated facially to one or two H(1) or H(2) protons in the supercages. The coordination to two protons has not been reported for the adsorption of benzene in any zeolite yet, to the best of our knowledge; it might be that the zeolite model used overestimates the importance of this 2H(1) site, but we are confident that in the absence of direct chemical interactions it exists. We also found some small adsorption onto the 12-membered ring windows, in accordance with IR data.¹⁸

Diffusion at very low temperature proceeds mainly by gliding or creeping along the supercage walls, with energy barriers ranging between 10 and 20 kJ mol⁻¹. The window crossing is no exception and proceeds via adsorption of benzene on a H(1) on one side of the window and gliding to the other side, with an activation energy that is not different from that of the intracage jumps. Cartwheel jumps between two sites are also possible, but with much higher activation energies reaching 30 kJ mol⁻¹. The energies reported here are in good agreement with the experimental data of Sousa-Gonçalves et al.²⁰ These authors report two activation energies, that is, 10 kJ mol⁻¹ at low temperature, and 25 kJ mol⁻¹ at high temperature, attributed to intracage and intercage jumps, respectively. Our simulation results suggest that there is no relation between these types of jumps and the activation energies; it might be that the difference observed originates in the large heterogeneity of the energies evidenced in our simulations.

The high Si/Al ratio of the model used implies that lots of H(1) and H(2) protons are available for benzene adsorption. As a consequence we observe multiple sites and multiple pathways between the sites. Even at low temperatures, "compound sites" made of two or more single sites are observed in the MC simulations. The notion of a site-to-site jump therefore loses the strict sense that it has, for example, in NaY. Note however that the notion of sites still makes sense, since they are stable at 200 K during a 20 ps molecular dynamics (MD) simulation, and since they appear on the umbrella sampling of a pathway between two supercages as positions with maximum probability of presence. Calculations of the dynamic rate constants between two sites inside the same cage show that it is the absence of any relaxation in the final site that destroys the site-to-site picture of intracage diffusion of benzene in HY. The same dynamic computations of the rate constants for the cage-to-cage jumps show, however, that the latter rates retain some physical meaning. The rates present an activation energy that confirms the heterogeneity found in the nondynamic calculations, and that are in global agreement with the experimental values.

The results presented here show that diffusion of benzene in HY, even at 200 K, should be regarded as a cage-to-cage mechanism with relaxation in the final cage, but without reference to particular adsorption sites. Such a model can easily be integrated in a KMC simulation.^{13,88} The rates for cage-to-cage jumps could in principle be calculated from unconstrained molecular dynamics calculations.^{88,89} Though this causes no problem at high enough temperature, the MD runs performed in this study show that at 200 K the benzene molecules remain in the stable adsorption sites for at least 20 ps. At low temperatures, very long calculations would be needed to find statistically averaged rates. However, such a procedure is probably needed in order to find out the loading dependence of the rates, essential for a KMC representation of the diffusion.

Acknowledgment. F.J. and D.P.V. wish to thank the FUNDP for the use of the Namur Scientific Computing Facility Center (SCF). They acknowledge financial support from the FNRS-FRFC, the "Loterie Nationale" for the convention no. 9.4595.96, and IBM Belgium for the Academic Joint Study on "Cooperative Processing for Theoretical Physics and Chemistry." F.J. acknowledges Prof. A. Lucas, Director of the PAI 4-10, for the attribution of a postdoctoral fellowship. S.M.A. gratefully acknowledges support from the US National Science Foundation under grants CHE-9616019 and CTS-9734153. F.J. and D.P.V. thank T. Latour for helpful discussions.

References and Notes

- (1) Demontis, P.; Yashonath, S.; Klein, M. L. *J. Phys. Chem.* **1989**, *93*, 5016.
- (2) Uytterhoeven, L.; Dompas, D.; Mortier, W. J. *J. Chem. Soc., Faraday Trans.* **1992**, *88*, 2753.
- (3) Auerbach, S. M.; Henson, N. J.; Cheetham, A. K.; Metiu, H. I. *J. Phys. Chem.* **1995**, *99*, 10 600.
- (4) Mosell, T.; Schrimpf, G.; Hahn, C.; Brickmann, J. *J. Phys. Chem.* **1996**, *100*, 4571.
- (5) Auerbach, S. M.; Bull, L. M.; Henson, N. J.; Metiu, H. I.; Cheetham, A. K. *J. Phys. Chem.* **1996**, *100*, 5923.
- (6) Klein, H.; Fuess, H.; Schrimpf, G. *J. Phys. Chem.* **1996**, *100*, 11 101.
- (7) Jousse, F.; Auerbach, S. M. *J. Chem. Phys.* **1997**, *107*, 9629.
- (8) Auerbach, S. M.; Metiu, H. I. *J. Chem. Phys.* **1996**, *105*, 3753.
- (9) Auerbach, S. M.; Metiu, H. I. *J. Chem. Phys.* **1997**, *106*, 2893.
- (10) Saravanan, C.; Auerbach, S. M. *J. Chem. Phys.* **1997**, *107*, 8120.
- (11) Saravanan, C.; Auerbach, S. M. *J. Chem. Phys.* **1997**, *107*, 8132.
- (12) Saravanan, C.; Jousse, F.; Auerbach, S. M. *J. Chem. Phys.* **1998**, *108*, 2162.
- (13) Saravanan, C.; Jousse, F.; Auerbach, S. M. *Phys. Rev. Lett.* **1998**, *80*, 5754.
- (14) Isfort, O.; Boddenberg, B.; Fujara, F.; Grosse, R. *Chem. Phys. Lett.* **1998**, *288*, 71.
- (15) Dzhigit, O. M.; Kiselev, A. V.; Rachmanova, T. A. *Zeolites* **1984**, *4*, 389.
- (16) Bull, L. M.; Cheetham, A. K.; Powell, B. M.; Ripmeester, J. A.; Ratcliffe, C. I. *J. Am. Chem. Soc.* **1995**, *117*, 4328.
- (17) Vitale, G.; Bull, L. M.; Powell, B. M.; Cheetham, A. K. *J. Chem. Soc., Chem. Commun.* **1995**, *22*, 2253.
- (18) Su, B.-L.; Barthomeuf, D. *J. Catal.* **1993**, *139*, 81.
- (19) Su, B.-L.; Barthomeuf, D. *Zeolites* **1993**, *13*, 626.
- (20) Sousa-Gonçalves, J. A.; Portsmouth, R. L.; Alexander, P.; Gladden, L. F. *J. Phys. Chem.* **1995**, *99*, 3317.
- (21) Beck, L. W.; Xu, T.; Nicholas, J. B.; Haw, J. F. *J. Am. Chem. Soc.* **1995**, *117*, 11 594.
- (22) June, R. L.; Bell, A. T.; Theodorou, D. N. *J. Phys. Chem.* **1991**, *95*, 8866.
- (23) Maginn, E. J.; Bell, A. T.; Theodorou, D. N. *J. Phys. Chem.* **1996**, *100*, 7155.
- (24) Chen, Y. D.; Yang, R. T. *AIChE J.* **1991**, *37*, 1579.
- (25) Chuan Kang, H.; Weinberg, W. H. *Chem. Rev.* **1995**, *95*, 667.
- (26) Meier, W. M.; Olson, D. H. *Atlas of Zeolite Structure Types*, 3rd rev. ed.; Butterworth-Heinemann: London, 1992.
- (27) Herrero, C. P. *J. Phys. Chem.* **1991**, *95*, 3282.
- (28) Klinowski, J.; Ramdas, S.; Thomas, J. M.; Fyfe, C. A.; Hartman, J. S. *J. Chem. Soc., Faraday Trans. 2* **1982**, *78*, 1025.
- (29) Olson, D. H.; Dempsey, E. *J. Catal.* **1969**, *13*, 221.
- (30) Jiráček, Z.; Vratislav, S.; Bosáček, V. *J. Phys. Chem. Solids* **1980**, *41*, 1089.
- (31) Czjzek, M.; Jobic, H.; Fitch, A. N.; Vogt, T. *J. Phys. Chem.* **1992**, *96*, 1535.
- (32) Bull, L. M.; Henson, N. J.; Cheetham, A. K.; Newsam, J. M.; Heyes, S. J. *J. Phys. Chem.* **1993**, *97*, 11 776.
- (33) Jacobs, P. A.; Uytterhoeven, J. B. *J. Chem. Soc., Faraday Trans.* **1973**, *169*, 359.
- (34) van Santen, R. A.; Kramer, G. J. *Chem. Rev.* **1995**, *95*, 637.
- (35) Jobic, H. *J. Catal.* **1991**, *131*, 289.
- (36) Schröder, K.-P.; Sauer, J.; Leslie, M.; Catlow, C. R. A.; Thomas, J. M. *Chem. Phys. Lett.* **1992**, *188*, 320.
- (37) Datka, J.; Gil, B. *J. Catal.* **1994**, *145*, 372.
- (38) Datka, J.; Broclawik, E.; Gil, B.; Sierka, M. *J. Chem. Soc., Faraday Trans.* **1996**, *92*, 4643.
- (39) Sierka, M.; Eichler, U.; Datka, J.; Sauer, J. *J. Phys. Chem. B* **1998**, *102*, 6397.
- (40) Barthomeuf, D.; Ha, B.-H. *J. Chem. Soc., Faraday Trans. 1* **1973**, *12*, 2147.

- (41) Barthelemy, D.; Ha, B.-H. *J. Chem. Soc., Faraday Trans. 1* **1973**, 12, 2158.
- (42) Suzuki, T.; Hirano, M.; Tamon, H.; Okazaki, M. *J. Phys. Chem.* **1995**, 99, 15 968.
- (43) Hunger, B.; Heuchel, M.; Matysik, S.; Beck, K.; Einicke, W. D. *Thermochimica Acta* **1995**, 269/270, 599.
- (44) Hunger, M.; Horvath, T. *J. Chem. Soc., Chem. Commun.* **1995**, 14, 1423.
- (45) Sarv, P.; Tuherm, T.; Lippmaa, E.; Keskinen, K.; Root, A. *J. Phys. Chem.* **1995**, 99, 13 763.
- (46) MSI Discover96.0 User Guide; San Diego, CA, 1996.
- (47) Bezus, A. G.; Kiselev, A. V.; Lopatkin, A. A.; Du, P. Q. *J. Chem. Soc., Faraday Trans.* **1978**, 2, 367.
- (48) Mellot, C. F.; Davidson, A. M.; Eckert, J.; Cheetham, A. K. *J. Phys. Chem. B* **1998**, 102, 2530.
- (49) Mellot, C. F.; Cheetham, A. K.; Harms, S.; Savitz, S.; Gorte, R. J.; Myers, A. L. *J. Am. Chem. Soc.* **1998**, 120, 5788.
- (50) Gale, J. D.; Henson, N. J. *J. Chem. Soc., Faraday Trans.* **1994**, 90, 3175.
- (51) Henson, N. J.; Cheetham, A. K.; Redondo, A.; Levine, S. M.; Newsam, J. M. In *Zeolites and Related Microporous Materials: State of the Art 1994* Weitkamp, J., Karge, H. G., Pfeifer, H., Hölderich, W., Eds.; Elsevier: Amsterdam, 1994; 2059.
- (52) van Beest, B. W. H.; Kramer, G. J.; van Santen, R. A. *Phys. Rev. Lett.* **1990**, 64, 1955.
- (53) Kramer, G. J.; Farragher, N. P.; van Beest, B. W. H.; van Santen, R. A. *Phys. Rev. B* **1991**, 43, 5068.
- (54) Jaramillo, E.; Auerbach, S. M. *J. Phys. Chem. B*, in press.
- (55) van Santen, R. A.; Neurock, M. *Catal. Rev.* **1995**, 37, 557.
- (56) Sauer, J. *Chem. Rev.* **1989**, 89, 199.
- (57) Suk, J. E.; No, K. T. *Bull. Korean Chem. Soc.* **1995**, 16, 915.
- (58) Janssens, G. O. A.; Baekelandt, B. G.; Toufar, H.; Mortier, W. J.; Schoonheydt, R. A. *J. Phys. Chem.* **1995**, 99, 3251.
- (59) Toufar, H.; Baekelandt, B. G.; Janssens, G. O. A.; Mortier, W. J.; Schoonheydt, R. A. *J. Phys. Chem.* **1995**, 99, 13 876.
- (60) Hill, J.-R.; Sauer, J. *J. Phys. Chem.* **1994**, 98, 1238.
- (61) Hill, J.-R.; Sauer, J. *J. Phys. Chem.* **1995**, 99, 9536.
- (62) Corma, A. *Chem. Rev.* **1995**, 95, 559.
- (63) Teunissen, E. H.; Jansen, A. P. J.; van Santen, R. A.; Orlando, R.; Dovesi, R. *J. Chem. Phys.* **1994**, 101, 5865.
- (64) Ghermani, N. E.; Lecomte, C.; Dusausoy, Y. *Phys. Rev. B* **1996**, 53, 5231.
- (65) Blake, N. P.; Weakliem, P. C.; Metiu, H. *J. Phys. Chem. B* **1998**, 102, 67.
- (66) Slater, J. C.; Kirkwood, J. G. *Phys. Rev.* **1931**, 37, 682.
- (67) Greengard, L.; Rokhlin, V. *J. Comput. Phys.* **1987**, 73, 325.
- (68) Wang, H. Y.; LeSar, R. *J. Chem. Phys.* **1996**, 104, 4173.
- (69) Henson, N. J.; Auerbach, S. M. *DIZZY Computational Chemistry Program*; 1994–1998.
- (70) Chandler, D. *J. Chem. Phys.* **1978**, 68, 2959.
- (71) Voter, A. F.; Doll, J. D. *J. Chem. Phys.* **1984**, 80, 5832.
- (72) Atkins, P. W. *Physical Chemistry, Fourth Edition*; Oxford University Press: Oxford, U.K., 1990.
- (73) Allen, M. P.; Tildesley, D. J. *Computer Simulations of Liquids*; Clarendon Press: Oxford, 1987.
- (74) Jousse, F.; Leherte, L.; Vercauteren, D. P. *J. Mol. Catal. A: Chemical* **1997**, 119, 165.
- (75) Saravanan, C.; Jousse, F.; Auerbach, S. M. In *Transition State Modeling for Catalysts* Truhlar, D. G., Morokuma, K., Eds.; 1999; p 296.
- (76) Frenkel, D.; Smit, B. *Understanding Molecular Simulations*; Academic Press: San Diego, CA, 1996.
- (77) Straatsma, T. P. In *Reviews in Computational Chemistry*; Lipkowitz, K. B., Boyd, D. B., Eds.; VCH: New York, 1996; Vol. 9, p 81.
- (78) Senderowitz, H.; Guarneri, F.; Still, W. C. *J. Am. Chem. Soc.* **1995**, 117, 8211.
- (79) Hummer, G.; Szabo, A. *J. Chem. Phys.* **1996**, 105, 2004.
- (80) Kong, X.; Brooks, C. L., III. *J. Chem. Phys.* **1996**, 105, 2414.
- (81) Kumar, S.; Wayne, P. W.; Vásquez, M. *J. Comput. Chem.* **1996**, 17, 1269.
- (82) den Otter, W. K.; Briels, W. J. *J. Chem. Phys.* **1998**, 109, 4139.
- (83) Sprik, M.; Ciccotti, G. *J. Chem. Phys.* **1998**, 109, 7737.
- (84) Voter, A. F. *J. Chem. Phys.* **1985**, 82, 1890.
- (85) Chandler, D. *Introduction to Modern Statistical Mechanics*; Oxford University Press: New York, 1987.
- (86) Hriljac, J. A.; Eddy, M. M.; Cheetham, A. K.; Donohue, J. A.; Ray, G. J. *J. Solid State Chem.* **1993**, 106, 66.
- (87) Mosell, T.; Schrimpf, G.; Brickmann, J. *J. Phys. Chem. B* **1997**, 101, 9476.
- (88) Jousse, F.; Auerbach, S. M.; Vercauteren, D. P. *J. Phys. Chem. B* **1998**, 102, 6507.
- (89) Jousse, F.; Leherte, L.; Vercauteren, D. P. *J. Phys. Chem. B* **1997**, 101, 4717.